NANO LETTERS

Letter

pubs.acs.org/NanoLett

Polymer Nanofiber-Guided Uniform Lithium Deposition for Battery Electrodes

Zheng Liang,[†] Guangyuan Zheng,[‡] Chong Liu,[†] Nian Liu,[†] Weiyang Li,[†] Kai Yan,[†] Hongbin Yao,[†] Po-Chun Hsu,[†] Steven Chu,[§] and Yi Cui*[,†,∥]

[†]Department of Materials Science and Engineering, [‡]Department of Chemical Engineering, and [§]Department of Physics, Stanford University, Stanford, California 94305, United States

[∥]Stanford Institute for Materials and Energy Sciences, SLAC National Accelerator Laboratory, 2575 Sand Hill Road, Menlo Park, California 94025, United States

Supporting Information

ABSTRACT: Lithium metal is one of the most promising candidates as an anode material for next-generation energy storage systems due to its highest specific capacity (3860 mAh/g) and lowest redox potential of all. The uncontrolled lithium dendrite growth that causes a poor cycling performance and serious safety hazards, however, presents a significant challenge for the realization of lithium metal-based batteries. Here, we demonstrate a novel electrode design by placing a three-dimensional (3D) oxidized polyacrylonitrile nanofiber network on top of the current collector. The polymer fiber with polar surface functional groups could guide the lithium ions to form uniform lithium metal deposits confined on the polymer fiber surface and in the 3D polymer layer. We showed stable cycling of lithium metal anode with an average Coulombic efficiency of 97.4% over 120 cycles in ether-based electrolyte at a current density of 3 mA/cm^2 for a total of 1 mAh/cm^2 of lithium.

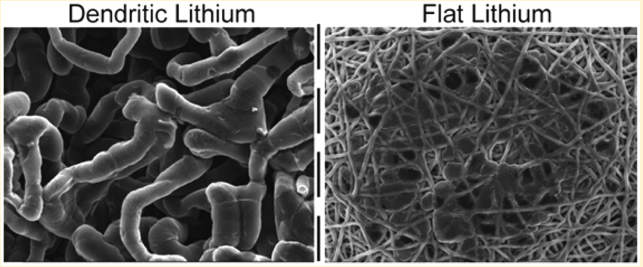

KEYWORDS: *Lithium metal anode, polymer fiber, Coulombic efficiency, uniform deposition, oxidized polyacrylonitrile*

High-performance rechargeable batteries are essential for meeting the demand for new energy storage applications. Secondary lithium ion battery (LIB) is receiving intense interest owing to its high energy density, high power density and long cycle life. Lithium (Li) metal is considered as the "Holy Grail" of battery technologies, as a result of its low gravimetric density (0.53 g/cm^3),[1] lowest redox potential (−3.04 V vs the standard hydrogen electrode), and high theoretical specific capacity (3860 mAh/g, 10 times that of commercial graphite anode).[1] Its specific capacity is even higher than the recently intensely studied anodes such as Si, Ge and Sn.[2−10] In addition, utilization of Li metal anodes eliminates the need for current collectors in conventional batteries with carbonaceous anodes, hence the total cell weight can be dramatically reduced. Therefore, Li metal could be a favorable candidate to be employed in highly promising, next-generation energy storage systems such as Li−Sulfur (Li−S) battery and Li−Air battery.

However, uncontrolled Li dendrite growth still remains as the most critical problem in widespread production and commercialization of Li metal-based cells. Because of its highly reactive nature, Li reacts spontaneously with most organic electrolyte solvents and Li salts to instantly form a solid electrolyte interphase (SEI) layer on the Li surface.[11] The SEI layer is ionically conductive but electrically insulating and thus can prevent further loss of Li and electrolyte. Nonetheless, SEI layer cannot withstand the mechanical deformation resulted from the Li-plating−stripping process, because of its brittleness.[12] Once a pinhole is formed in the SEI layer, as schematically summarized in Figure 1a, the fresh Li underneath would be exposed to the electrolyte. Upon electrochemical cycling, Li ions then diffuse toward the defect and concentrate in the vicinity, creating the so-called "hot spots". It is well recognized that Li dendrite growth is accelerated at these hot spots where the current density is locally enhanced dramatically.[13] The resulting treelike Li metal dendrite will pierce through the separator and provoke internal short circuits, posing a significant safety hazard.[14−17] In addition, owing to the large surface area and high chemical reactivity of Li dendrite, there is continuous consumption of Li and electrolyte through the formation/dissolution of SEI[18] over repeated Li-plating−stripping processes, giving rise to a low Coulombic efficiency. Thereby, excess Li is required to compensate the Li loss.

To address the aforementioned issues, most efforts were related to reinforcing and stabilizing the SEI layer by adding various electrolyte additives, including hydrogen fluoride (HF),[19,20] vinylene carbonate (VC),[21,22] fluoroethylene carbonate (FEC),[23] tetraethoxysilane (TEOS),[24] 2-methylfuran (2Me-F),[25,26] toluene,[27,28] and metal ions.[29,30] These functional additives react quickly with Li through decomposition/

Received: December 2, 2014
Revised: March 9, 2015
Published: March 30, 2015

DOI: 10.1021/nl5046318
Nano Lett. 2015, 15, 2910−2916

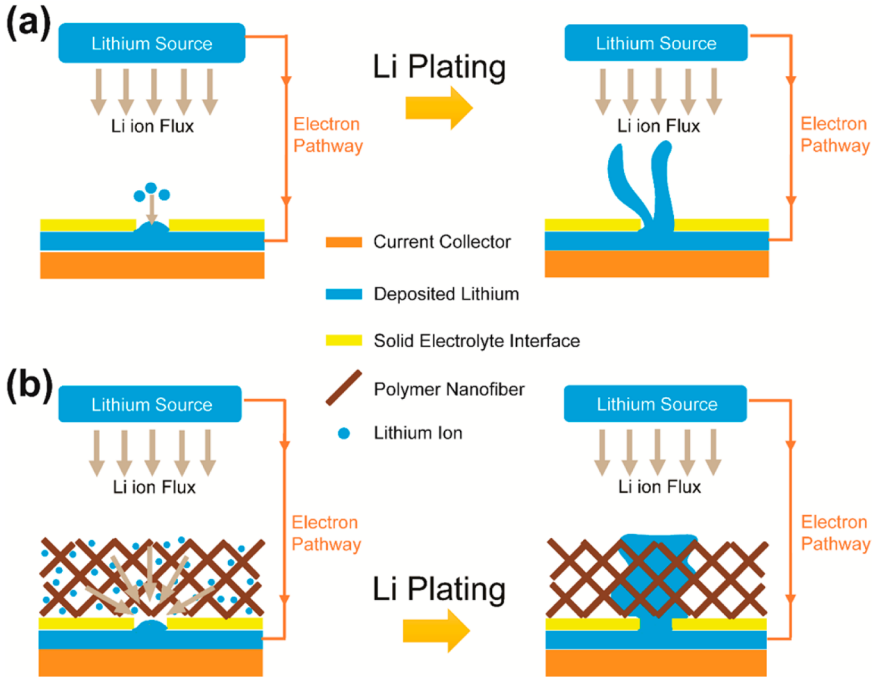

Figure 1. Schematic diagrams of Li deposition. (a) Schematics showing Li deposition on bare Cu electrode. Li ions concentrate in the vicinity of the dendrite tip, which leads to a mossy Li growth and severe electrolyte decomposition. (b) Modifying the Cu electrode with a layer of polymer nanofiber network triggers a homogeneous Li deposition and less electrolyte consumption.

adsorption/polymerization and generate a protective layer on the Li metal surface, which helps enhance the SEI. However, the mechanical strength of these in situ formed protective films is not high enough to withstand the large volume change during the process of Li deposition and dissolution. Moreover, the physical cohesion of these thin films onto Li metal is very limited.[13] Therefore, suppression of dendritic formation by electrolyte additives is not sustainable. Instead of improving stability of the intrinsic SEI layer, recently, we have successfully shown the employment of interconnected hollow carbon spheres[31] and hexagonal boron nitride[32] as promising artificial SEI layers. These artificial SEI layers are mechanically strong and chemically stable. We showed that they effectively block Li metal dendrite growth and improve the cycling Coulombic efficiency by maintaining a stable interface between the Li and electrolyte.

While numerous studies have focused on the interface of Li metal and the electrolyte, by either strengthening the intrinsic SEI or building a new interfacial layer, it transpires that Li dendrite growth originates mainly from the spatial inhomogeneity in charge distribution over the entire electrode surface.[11,13,33] To prevent the Li dendrite growth from the origin, uniform distribution of ionic flux needs to be achieved. Along this line, we demonstrate a novel electrode design by placing a 3D oxidized polyacrylonitrile (PAN) nanofiber layer on top of the current collector. The polar functional groups on the polymer nanofiber surface serve as the adhesion sites to bind with Li ions in the electrolyte. As a result, during electrochemical cycling, the movement of Li ions toward the "hot spots" is retarded by the attraction force from polymer fiber functional groups, facilitating a relatively homogeneous Li ionic flux (Figure 1b). Moreover, the polar surface groups of polymer nanofiber mat have good affinity with electrolyte. It ensures a larger amount of electrolyte uptake and a better electrode–electrolyte contact (compared with conventional polyethylene separator only). Furthermore, the electrically insulating polymer is not involved in the Li deposition although it could play the role of a 3D scaffold to guide and confine the growth of Li along the fiber because the polar surface functional groups have a strong affinity with Li metal. We expect that the resulting Li has a planar morphology embedded inside the nanofiber matrix, as illustrated by the gray region in Figure 1b. In addition, the oxidized PAN exhibits excellent chemical stability toward electrochemical cycling in a highly reducing environment.

Results and Discussion. We developed a simple two-step process to fabricate the polymer nanofiber network (Supporting Information Figure S1). The precursor solution for our polymer nanofiber was made by adding polyacrylonitrile (PAN) and polyvinylpyrrolidone (PVP) into *N*,*N*-Dimethylformamide (DMF) with vigorous stirring (Supporting Information Figure S1a). Afterward, we utilize a single-nozzle coelectrospinning method to produce the PAN/PVP nonwoven polymer nanofiber mat. The as-prepared precursor solution was injected from a 2 mL syringe and electrospun onto the collector under a constant voltage (Supporting Information Figure S1b). Then the nanofiber mat was transferred to a box furnace and heated at elevated temperature (300 °C) to slightly oxidize the PAN/PVP hybrid nanofiber (detailed experimental methods in Supporting Information). PAN is used as the starting material for our nanofiber synthesis owing to its availability and polar nitrile groups on the side chain.[34] PVP is introduced to the electrospinning process as a functional additive for modulating the fiber morphology in order to maintain the fiber uniformity.[35,36] These two polymers phase segregate and form a core–shell structure (PAN as the core and PVP as the shell) during the electrospinning process in that they possess different intrinsic properties such as viscosities.[35,37] Afterward, PVP shell might be removed completely by thermal decomposition in the following stabilization step[34,38−40] due to

DOI: 10.1021/nl5046318
Nano Lett. 2015, 15, 2910−2916

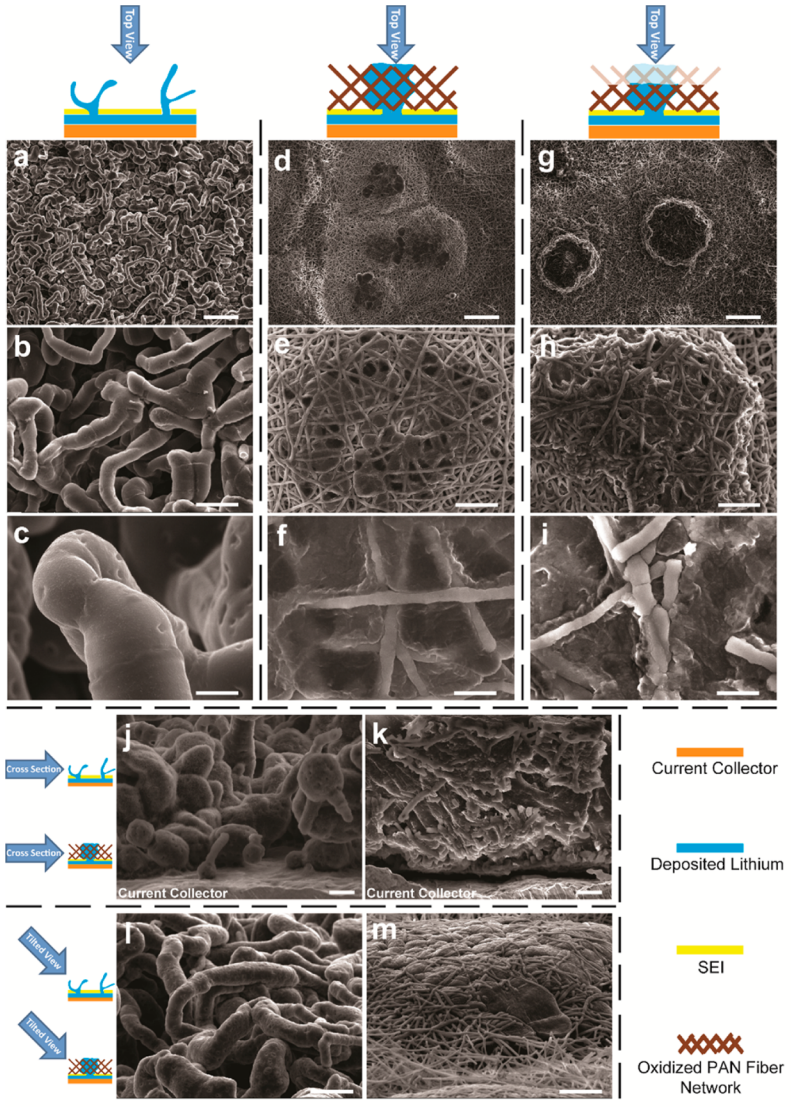

Figure 2. Morphology study of Li deposition on Cu electrode and Cu-OxPAN electrode with current density of 3 mA/cm^2 for a total of 3 mAh/cm^2 of Li. (a–c) Top-view SEM images of ramified growth of dendritic Li on bare Cu electrode. (d–f) Top-view SEM images of Li deposition on Cu-OxPAN electrode showing the smooth Li surface. (g–i) Top-view SEM images of the internal structure of Li deposition on Cu-OxPAN electrode after removing the top layer. (j,k) Comparison of cross-sectional SEM images of Li deposition on bare Cu and Cu-OxPAN electrode; Li filaments are protruding upward on bare Cu electrode without any confinement. (l,m) Comparison of tilted-view SEM images of Li deposition on bare Cu and Cu-OxPAN. The growth of Li is confined within the polymer fiber layer. Scale bars in (a,d,g) are 20 μm. Scale bars in (b,e,h) are 5 μm. Scale bars in (c,f,i) are 1 μm. Scale bars in (j,k) and (l,m), are 2 and 5 μm, respectively.

its low melting temperature and thermoplasticity.[39] Alternatively, it is also possible to leave some C═O and C–N containing chemical fragments on the fiber surface.[38] In summary, PVP is added to assist the electrospinning only and has little influence on the Li deposition (detailed discussion in Supporting Information Figure S2).

The thermal stabilization process involves annealing the polymer fiber at a moderately high temperature of 300 °C in air (Supporting Information Figure S1c). According to the statistical analysis (Supporting Information Figures S3 and S4), the pristine PAN/PVP nanofiber shows a uniform morphology with an average diameter of 288 ± 27 nm (Supporting Information Figure S3a). The PAN/PVP fiber displays a relatively narrow diameter distribution compared with PAN nanofiber without the addition of PVP (256 ± 55 nm, Supporting Information Figure S4a). The shrinkage in the fiber diameter before (288 nm in average) and after (193 nm in average) oxidation may be ascribed to the thermal degradation of the outer layer PVP (Supporting Information Figure S3a, S3c). In the oxidation/stabilization stage, PAN undergoes a cyclization-oxidation reaction and form a ladder structure with polar functional groups (C═N, C–N, C═O, O–H) working as anchoring points for Li ions (Supporting Information Figure S1c). The stabilization step plays a key role since it helps eliminate the residues (organic solvents and water) remained in the nanofiber mat.[34] The as-formed cross-linked PAN fiber has an improved chemical stability in the electrolyte, ensuring little swelling and side reactions during the Li-plating–stripping cycles (Supporting Information Figure S3c, S 3d). After the stabilization process, the oxidized PAN nanofiber could be easily detached from the collector and become a free-standing, mechanically strong film. The calculated fiber layer porosity is 85% (Supporting Information Figure S5). The nanofiber mat was cut into 1 cm^2 and then placed on top of Li metal foils or

DOI: 10.1021/nl5046318
Nano Lett. 2015, 15, 2910–2916

copper (Cu) current collectors to individually form two new hybrid electrode structures. These two thus formed hybrid electrodes are denoted as Li-OxPAN or Cu-OxPAN, respectively.

SEM characterization was performed on the deposited Li. Figure 2a−c presents the top-view SEM images of deposited Li on bare Cu (control cell) at different magnifications. After direct deposition of Li at current density of 3 mA/cm^2 for 1 h, the top surface of the as-grown Li shows a nonuniform structure with long Li filaments. The cross-sectional and tilted view of the as-deposited Li on bare Cu again confirm the uneven morphology and overgrowth of Li filaments (Figure 2j,l). The dendrites could be observed clearly with a diameter of ∼2 μm. In contrast, Li deposition onto modified Cu-OxPAN electrode displays a drastic change in morphology. The top-view images illustrate that pancake-like Li is created at the same experimental condition with the control cell (Figure 2d−f). The flat and uniform Li is embedded inside the polymer nanofiber layer, and Li tends to fulfill the opening space between each single fiber. The 3D polymer nanofiber network hinders Li ions from concentrating around the "hot spots", enabling a relatively homogeneous current distribution and facilitating the uniform growth of the Li. At the top frontier of the fiber mat, Li is evenly distributed, forming a smooth layer. No dendrite is observed protruding upward which addresses the potential safety problem (Figure 2m). In order to observe the Li distribution inside the polymer fiber network, the top part of the fiber layer was removed by Scotch tape, as presented in Figure 2g−i. The lithium beneath exhibits a dense and solid structure that promotes a much smaller surface area compared to the dendritic lithium without any confinement.[31] The cross-sectional image provides additional evidence, suggesting Li deposition was confined within layer of the polymer fibers (Figure 3k). To investigate the significance of the polar functional groups of nanofiber, nonpolar polypropylene (PP) fiber layer was coated on Cu electrode (Cu-PP) as a comparison. Morphology of Li deposition on Cu-PP electrode was studied (Supporting Information Figure S6). The as-made Cu-PP electrode displays a ramified growth of Li, as a consequence of the weak interactions between Li ions and the nonpolar CH_3 groups.

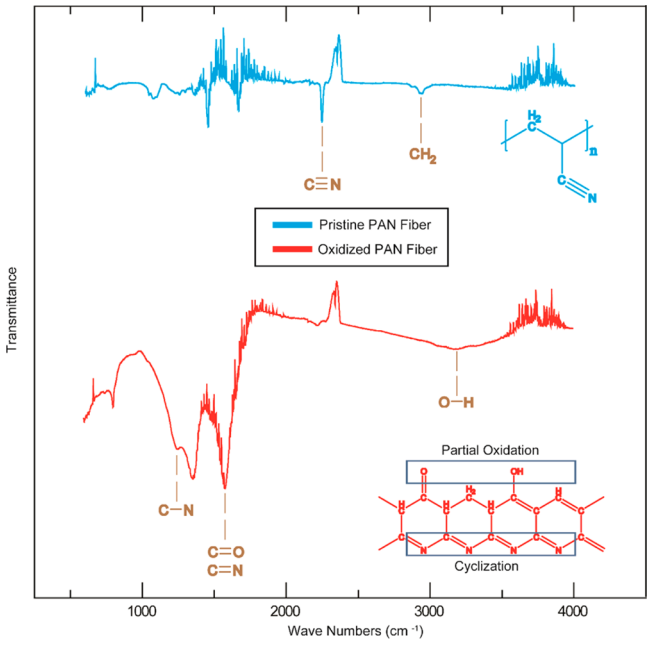

Figure 3. FTIR of pristine PAN fiber and oxidized PAN fiber. The proposed mechanism for PAN oxidization consists of cyclization of nitrile groups and partial oxidation. The oxidized PAN exhibits a cross-linked structure with polar functional groups on the side chain.

Fourier transform infrared spectrometry (FTIR) is used to explore the component change and functional groups on the polymer nanofiber after thermal stabilization (300 °C in air). As illustrated in Figure 3, the spectrum of pure PAN fiber before stabilization exhibits typical PAN absorbance peaks: saturated nitrile group at 2245 cm^{-1}[41−43] and aliphatic C−H bonds around 2940 cm^{-1}.[43,44] After thermal stabilization, a new broad peak centered at 3200 cm^{-1} is created owing to the OH group formation.[31] The absorption in the range of 1250−1265 cm^{-1} is attributed to C−N group.[41,44] Strong band within the region of 1580−1650 cm^{-1} is related to the mixed modes of resonance of C═O bond and C═N bond.[41,44−46] The polymer undergoes a series of structural change during the thermal stabilization at 300 °C with the proposed chemical formula of oxidized PAN shown in Figure 3. The main stabilization mechanism is complex and consists of two reactions: cyclization and partial oxidation.[43,45] According to the FTIR spectra of PAN before and after stabilization, it could be seen clearly that the bands at 2245 cm^{-1} (C≡N) decrease drastically in intensity, along with conjugated C═N and C−N formed instead. This elucidates a reduction of nitrile groups induced by intermolecular cross-linking or intramolecular cyclization.[42,46] The appearance of the peaks for OH and C═O after stabilization is possibly related to the incorporation of oxygen.[46] Taken these together, the thermal stabilization of PAN involves cyclization of nitrile groups followed by oxygen intake, leading to the formation of a chemically stable structure with functional groups of high polarities (O−H, C═O, C−N). Moreover, the absence of PVP in oxidized PAN/PVP fiber was confirmed in Supporting Information Figure S7.

To study the overall electrochemical performances of our new design of Li metal anodes, we conducted the galvanostatic cycling test with ether-based electrolyte. Cells with modified electrode and control electrode were compared in terms of Coulombic efficiency (Figure 4a), voltage profile (Figure 4b), and hysteresis (Figure 4c). Coin cells were assembled by using metallic Li foil as the counter electrode, Cu foil (control), and Cu-OxPAN (modified) as the working electrode. Lithium bis(trifluoromethanesulfonyl)imide (LiTFSI) in cosolvent of 1,3-dioxolane (DOL) and 1,2-dimethoxyethane (DME) with lithium nitrate (2 wt %) was used as electrolyte. Coulombic efficiency is an important consideration because it directly measures the quantity of Li metal consumption due to the reaction with electrolyte. Thus, it has great impact on the cycle life of a Li metal-based battery. In the coin cells we constructed, a fixed amount (1 mAh/cm^2) of Li was first plated onto bare Cu or Cu-OxPAN from the Li foil counter electrode. Then we strip the as-deposited Li away. We define the Coulombic efficiency to be a ratio of the amount of Li stripped back versus the total amount of Li plated onto the working electrode each cycle. Because the counter side always has excess Li, the Coulombic efficiency actually reflects the Li loss on the working electrode. As we can see from Figure 4a, the modified electrode presents a more stable electrochemical cycling and a longer cell life. Under current density of 1 and 3 mA/cm^2, the cells with modified electrodes deliver enhanced Coulombic efficiency of 97.9 and 97.4% over 120 cycles, respectively. In comparison,

DOI: 10.1021/nl5046318
Nano Lett. 2015, 15, 2910−2916

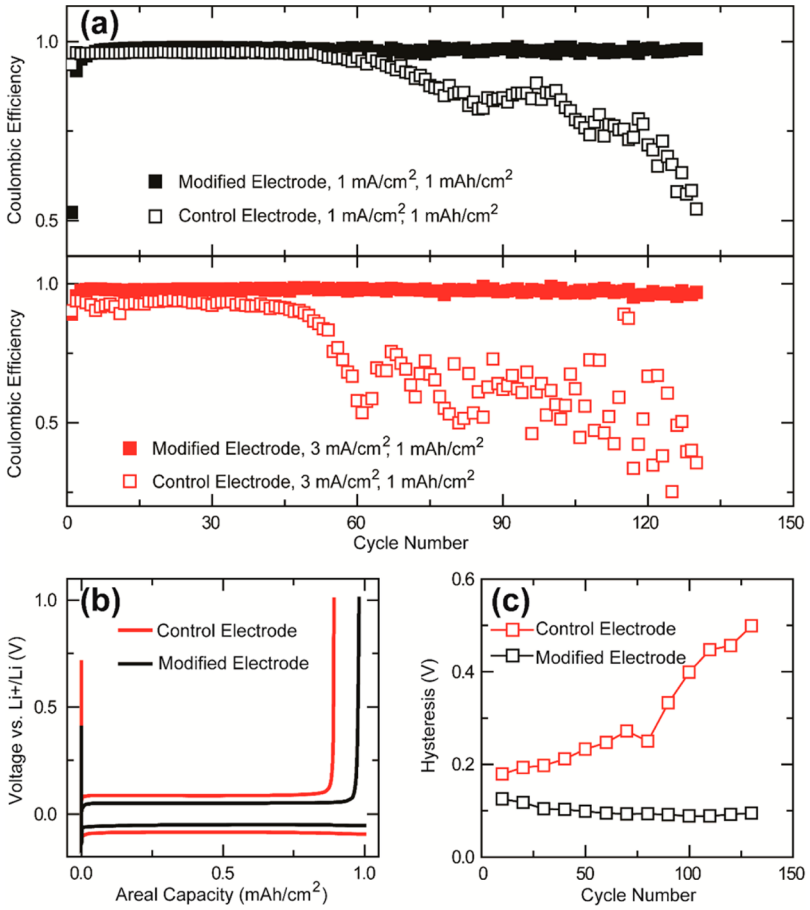

Figure 4. Cycling performances of the control Cu electrode and modified Cu-OxPAN electrode at various current rates. (a) Comparison of the Coulombic efficiency of Li deposition on bare Cu and Cu-OxPAN electrode with current densities of 1 mA/cm^2 and 3 mA/cm^2. The amount of Li plated in each cycle is 1 mAh/cm^2. (b) Comparison of the voltage profiles of the Li plating/stripping process with Li metal as the counter and reference electrode with current density of 3 mA/cm^2. (c) Comparison of voltage hysteresis of the Li plating/stripping process with Li metal as the counter and reference electrode with current density of 3 mA/cm^2.

the cells with control electrodes exhibits inferior electrochemical cycling performances with an average of 87.6% over 120 cycles (for 1 mA/cm^2) and 71.3% over 120 cycles (for 3 mA/cm^2). The Coulombic efficiencies of control electrodes drop to below 70% after 90 cycles (at 1 mA/cm^2) and 60 cycles (at 3 mA/cm^2), which indicates the depletion of the electrolyte resulted from the intense reaction of Li and electrolyte.[31] The observed low first cycle Coulombic efficiency for the modified electrode under 1 mA/cm^2 is possibly ascribed to the irreversible interaction between fiber surface functional groups and Li ions. The Cu-OxPAN electrode also shows improved cycling performance at high areal capacity (3 mAh/cm^2, Supporting Information Figure S8). The stable cycling of modified cells with Cu-OxPAN electrode even under large current density (3 mA/cm^2) originates from a homogeneous Li growth, thus a less Li and electrolyte consumption.[47,48] Electrochemical characterization of Li deposition on Cu-PP electrode (with nonpolar CH_3 groups) was also performed (Supporting Information Figure S6). The Cu-PP electrode presents a rapid Coulombic efficiency decay, which confirms the importance of polar functional groups.

Figure 4b depicts the voltage profile of Li-plating−stripping process. The Li plating voltage is approximately −50 mV (versus Li/Li$^+$) for modified electrode and −85 mV (versus Li/Li$^+$) for control electrode. The Li stripping voltage is 49 mV (versus Li/Li$^+$) for modified electrode and 86 mV (versus Li/Li$^+$) for control electrode (Figure 4b). The reduction in the overpotential of the modified electrode during Li plating and stripping could be seen clearly from the voltage profile. We define voltage hysteresis as the sum of the over potential for Li deposition and Li dissolution. The voltage hysteresis versus cycle numbers is also plotted in Figure 4c. The control electrode has a steadily increasing internal resistance during the electrochemical cycling, demonstrating a large hysteresis of ∼300 mV after 80 cycles, while the hysteresis of modified electrode is maintained at ∼75 mV over 80 cycles. The smaller hysteresis of modified electrode is attributed to the uniform Li deposition. This uniform Li would have smaller surface area compared to the mossy Li formed on the control electrode that leads to thinner SEI accumulated over the electrode surface during cycles and therefore a trivial cycling overpotential.

Interfacial stability and charge transfer behavior were investigated by assembling symmetrical coin cells with two identical Li metal sheets as the electrodes (detailed experimental methods in Supporting Information).[49] Bare Li foil was defined as the control electrode (Figure 5a) while Li-OxPAN was regarded as the modified electrode (Figure 5b). Upon cycling, 1 mAh/cm^2 of Li was electrochemically deposited back and forth between the two electrodes at a high current density of 3 mA/cm^2. Voltage profile was plotted

DOI: 10.1021/nl5046318
Nano Lett. 2015, 15, 2910−2916

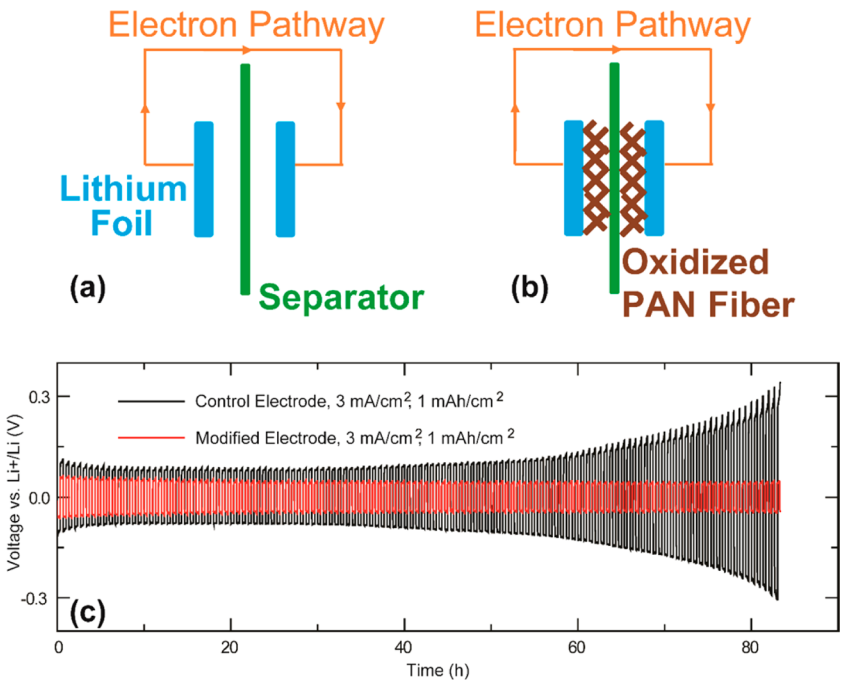

Figure 5. Symmetrical cell testing of bare Li electrode and Li-OxPAN electrode. (a) Schematics of the control cell design. (b) Schematics of the modified cell design. (c) Comparison of voltage profiles of the Li plating/stripping process at current density of 3 mA/cm^2. The amount of Li plated in each cycle is 1 mAh/cm^2.

versus cycling time (Figure 5c). Negative voltage value refers to the Li plating, while positive voltage value refers to the Li stripping (Figure 5c). In the initial stage, the cell with modified electrodes shows a smaller overpotential, which is related to the larger amount of electrolyte uptake and better electrode−electrolyte contact, owing to the introduction of the highly polar polymer fiber layer. For the control electrode, the voltage hysteresis keeps increasing with increasing cycle time. This is mainly ascribed to the nonuniform Li deposition and severe electrolyte decomposition, which leads to a gradually accumulated thick SEI layer. The hysteresis increases during each cycle and reaches its maximum when the electrolyte is totally depleted, as depicted in Figure 5c after 80 h. In comparison, the modified electrode displays a much lower voltage fluctuation, indicating a uniform Li growth with a stable and thin SEI, causing superior charge transfer kinetics. Because there is less electrolyte consumed from reactions with Li every cycle, the modified electrode has an enhanced cycle life than the control electrode.[50] To exclude the influence of $LiNO_3$ on the electrochemical performance, symmetrical cell testing was also conducted in electrolyte (1 M LiTFSI in DOL/DME) without $LiNO_3$, the modified Li-OxPAN electrode exhibits improved cycling stability (Supporting Information Figure S9). To further confirm the electrochemical stability of the polymer fiber network, X-ray photoelectron spectroscopy (XPS) characterization was conducted on the oxidized PAN nanofiber before and after cycling (Supporting Information Figure S10).

Conclusion. In conclusion, we have demonstrated the stable cycling of Li metal anodes by using a chemically inert and electronically insulating oxidized PAN nanofiber mat as a scaffold to guide and confine the deposition of Li. The polymer network allows homogeneous Li deposition embedded inside the 3D network via attraction forces between the polar functional groups and Li ions. The resulting Coulombic efficiency could reach 97.4% up to a practical current density of 3 mA/cm^2 and with an areal capacity of 1 mAh/cm^2 over more than 120 cycles in DOL/DME electrolyte. The stratagem of utilizing special designed 3D polymer nanofiber mat to address the uncontrolled Li dendrite growth problem would not only enable a series of Li metal-based energy storage technologies but also benefit general metal electrodeposition processes that are widely used in chemical industry.

■ ASSOCIATED CONTENT

Supporting Information

Schematics of the fabrication processes of the polymer nanofiber, SEM characterization and cycling performance of Li deposition on Cu-OxPAN* electrode, statistics of the polymer fiber diameter distribution, SEM characterization and cycling performance of Li deposition on Cu-OxPAN electrode and Cu-PP electrode, high areal capacity electrochemical cycling, statistics of the oxidized PAN fiber porosity distribution, electrochemical testing in electrolyte without $LiNO_3$, XPS study of oxidized PAN fiber before and after cycling, experimental details of polymer fiber fabrication, characterizations, electrochemical testing, and volumetric specific capacity calculation. This material is available free of charge via the Internet at http://pubs.acs.org.

■ AUTHOR INFORMATION

Corresponding Author

*E-mail: yicui@stanford.edu.

Author Contributions

Z.L. and G.Z. contributed equally to this work.

Notes

The authors declare no competing financial interest.

■ ACKNOWLEDGMENTS

Y.C. acknowledges the support from the Assistant Secretary for Energy Efficiency and Renewable Energy, Office of Vehicle

DOI: 10.1021/nl5046318
Nano Lett. 2015, 15, 2910−2916

Technologies of the U.S. Department of Energy. G.Z. acknowledges financial support from Agency for Science, Technology, and Research (A*STAR), Singapore.

REFERENCES

(1) Xu, W.; Wang, J.; Ding, F.; Chen, X.; Nasybulin, E.; Zhang, Y.; Zhang, J. G. *Energy Environ. Sci.* **2014**, *7*, 513.
(2) Lee, K. T.; Jung, Y. S.; Oh, S. M. *J. Am. Chem. Soc.* **2003**, *125*, 5652.
(3) Chan, C. K.; Peng, H.; Liu, G.; McIlwrath, K.; Zhang, X. F.; Huggins, R. A.; Cui, Y. *Nat. Nanotechnol.* **2008**, *3*, 31.
(4) Wang, C.; Wu, H.; Chen, Z.; McDowell, M. T.; Cui, Y.; Bao, Z. *Nat. Chem.* **2013**, *5*, 1042.
(5) Wu, H.; Cui, Y. *Nano Today* **2012**, *7*, 414.
(6) Yao, Y.; Liu, N.; McDowell, M. T.; Pasta, M.; Cui, Y. *Energy Environ. Sci.* **2012**, *5*, 7927.
(7) Wu, H.; Chan, G.; Choi, J. W.; Ryu, I.; Yao, Y.; McDowell, M. T.; Lee, S. W.; Jackson, A.; Yang, Y.; Hu, L.; Cui, Y. *Nat. Nanotechnol.* **2012**, *7*, 310.
(8) Yao, Y.; McDowell, M. T.; Ryu, I.; Wu, H.; Liu, N.; Hu, L.; Nix, W. D.; Cui, Y. *Nano Lett.* **2011**, *11*, 2949.
(9) Liu, N.; Lu, Z.; Zhao, J.; McDowell, M. T.; Lee, H.-W.; Zhao, W.; Cui, Y. *Nat. Nanotechnol.* **2014**, *9*, 187.
(10) Chan, C. K.; Zhang, X. F.; Cui, Y. *Nano Lett.* **2007**, *7*, 307.
(11) Kim, H.; Jeong, G.; Kim, Y.-U.; Kim, J.-H.; Park, C.-M.; Sohn, H.-J. *Chem. Soc. Rev.* **2013**, *42*, 9011.
(12) Lu, Y.; Das, S. K.; Moganty, S. S.; Archer, L. A. *Adv. Mater.* **2012**, *24*, 4430.
(13) Aurbach, D.; Zinigrad, E.; Cohen, Y.; Teller, H. *Solid State Ionics* **2002**, *148*, 405.
(14) Bhattacharyya, R.; Key, B.; Chen, H.; Best, A. S.; Hollenkamp, A. F.; Grey, C. P. *Nat. Mater.* **2010**, *9*, 504.
(15) Chandrashekar, S.; Trease, N. M.; Chang, H. J.; Du, L.-S.; Grey, C. P.; Jerschow, A. *Nat. Mater.* **2012**, *11*, 311.
(16) Harry, K. J.; Hallinan, D. T.; Parkinson, D. Y.; MacDowell, A. A.; Balsara, N. P. *Nat. Mater.* **2014**, *13*, 69.
(17) Lu, Y.; Korf, K.; Kambe, Y.; Tu, Z.; Archer, L. A. *Angew. Chem., Int. Ed.* **2014**, *53*, 488.
(18) Xu, K. *Chem. Rev.* **2004**, *104*, 4303.
(19) Shiraishi, S.; Kanamura, K.; Takehara, Z. i. *J. Electrochem. Soc.* **1999**, *146*, 1633.
(20) Takehara, Z.-i. *J. Power Sources* **1997**, *68*, 82.
(21) Stark, J. K.; Ding, Y.; Kohl, P. A. *J. Electrochem. Soc.* **2011**, *158*, A1100.
(22) Lane, G. H.; Best, A. S.; MacFarlane, D. R.; Forsyth, M.; Hollenkamp, A. F. *Electrochim. Acta* **2010**, *55*, 2210.
(23) Mogi, R.; Inaba, M.; Jeong, S.-K.; Iriyama, Y.; Abe, T.; Ogumi, Z. *J. Electrochem. Soc.* **2002**, *149*, A1578.
(24) Umeda, G. A.; Menke, E.; Richard, M.; Stamm, K. L.; Wudl, F.; Dunn, B. *J. Mater. Chem.* **2011**, *21*, 1593.
(25) Abraham, K. M.; Foos, J. S.; Goldman, J. L. *J. Electrochem. Soc.* **1984**, *131*, 2197.
(26) Bedenbaugh, A. O.; Bedenbaugh, J. H.; Adkins, J. D.; Bergin, W. A. *J. Org. Chem.* **1970**, *35*, 543.
(27) Saito, K.; Nemoto, Y.; Tobishima, S.; Yamaki, J. *J. Power Sources* **1997**, *68*, 476.
(28) Choi, J.-W.; Cheruvally, G.; Kim, D.-S.; Ahn, J.-H.; Kim, K.-W.; Ahn, H.-J. *J. Power Sources* **2008**, *183*, 441.
(29) Ishikawa, M.; Morita, M.; Matsuda, Y. *J. Power Sources* **1997**, *68*, 501.
(30) Ishikawa, M.; Yoshitake, S.; Morita, M.; Matsuda, Y. *J. Electrochem. Soc.* **1994**, *141*, L159.
(31) Zheng, G.; Lee, S. W.; Liang, Z.; Lee, H.-W.; Yan, K.; Yao, H.; Wang, H.; Li, W.; Chu, S.; Cui, Y. *Nat. Nanotechnol.* **2014**, *9*, 618.
(32) Yan, K.; Lee, H.-W.; Gao, T.; Zheng, G.; Yao, H.; Wang, H.; Lu, Z.; Zhou, Y.; Liang, Z.; Liu, Z.; Chu, S.; Cui, Y. *Nano Lett.* **2014**, *14*, 6016.
(33) Girishkumar, G.; McCloskey, B.; Luntz, A. C.; Swanson, S.; Wilcke, W. *J. Phys. Chem. Lett.* **2010**, *1*, 2193.
(34) Yao, H.; Zheng, G.; Hsu, P.-C.; Kong, D.; Cha, J. J.; Li, W.; Seh, Z. W.; McDowell, M. T.; Yan, K.; Liang, Z.; Narasimhan, V. K.; Cui, Y. *Nat. Commun.* **2014**, *5*, 3943.
(35) Lee, J. S.; Kwon, O. S.; Park, S. J.; Park, E. Y.; You, S. A.; Yoon, H.; Jang, J. *ACS Nano* **2011**, *5*, 7992.
(36) Wan, L.-S.; Xu, Z.-K.; Wang, Z.-G. *J. Polym. Sci., Part B: Polym. Phys.* **2006**, *44*, 1490.
(37) Bazilevsky, A. V.; Yarin, A. L.; Megaridis, C. M. *Langmuir* **2007**, *23*, 2311.
(38) Borodko, Y.; Lee, H. S.; Joo, S. H.; Zhang, Y.; Somorjai, G. *J. Phys. Chem. C* **2009**, *113*, 1117.
(39) Peniche, C.; Zaldívar, D.; Pazos, M.; Páz, S.; Bulay, A.; Román, J. S. *J. Appl. Polym. Sci.* **1993**, *50*, 485.
(40) Borodko, Y.; Habas, S. E.; Koebel, M.; Yang, P.; Frei, H.; Somorjai, G. A. *J. Phys. Chem. B* **2006**, *110*, 23052.
(41) Zhang, Z.; Li, X.; Wang, C.; Fu, S.; Liu, Y.; Shao, C. *Macromol. Mater. Eng.* **2009**, *294*, 673.
(42) Mittal, J.; Bahl, O. P.; Mathur, R. B.; Sandle, N. K. *Carbon* **1994**, *32*, 1133.
(43) Usami, T.; Itoh, T.; Ohtani, H.; Tsuge, S. *Macromolecules* **1990**, *23*, 2460.
(44) Kakida, H.; Tashiro, K. *Polym. J.* **1998**, *30*, 463.
(45) Shimada, I.; Takahagi, T.; Fukuhara, M.; Morita, K.; Ishitani, A. *J. Polym. Sci., Part A: Polym. Chem.* **1986**, *24*, 1989.
(46) Wangxi, Z.; Jie, L.; Gang, W. *Carbon* **2003**, *41*, 2805.
(47) Murugan, R.; Thangadurai, V.; Weppner, W. *Angew. Chem., Int. Ed.* **2007**, *46*, 7778.
(48) Thangadurai, V.; Narayanan, S.; Pinzaru, D. *Chem. Soc. Rev.* **2014**, *43*, 4714.
(49) Lu, Y.; Tu, Z.; Archer, L. A. *Nat. Mater.* **2014**, *13*, 961.
(50) Aurbach, D.; Zinigrad, E.; Teller, H.; Dan, P. *J. Electrochem. Soc.* **2000**, *147*, 1274.

DOI: 10.1021/nl5046318
Nano Lett. 2015, 15, 2910−2916